AGU PUBLICATIONS

JGR

Journal of Geophysical Research: Solid Earth

RESEARCH ARTICLE
10.1002/2016JB013263

Effect of particle entrainment on the runout of pyroclastic density currents

Kristen E. Fauria[1], Michael Manga[1], and Michael Chamberlain[1,2]

[1]Department of Earth and Planetary Science, University of California, Berkeley, California, USA, [2]Department of Civil and Environmental Engineering, University of California, Berkeley, California, USA

Key Points:
- Particle entrainment is quantified with an expression for particle splash
- Particle entrainment by splash increases runout distance
- Currents that entrain cold particles run out farther than those that entrain hot particles

Correspondence to:
K. E. Fauria,
kfauria@berkeley.edu

Citation:
Fauria, K. E., M. Manga, and M. Chamberlain (2016), Effect of particle entrainment on the runout of pyroclastic density currents, *J. Geophys. Res. Solid Earth*, *121*, doi:10.1002/2016JB013263.

Received 13 JUN 2016
Accepted 27 AUG 2016
Accepted article online 3 SEP 2016

Abstract Pyroclastic density currents (PDCs) can erode soil and bedrock, yet we currently lack a mechanistic understanding of particle entrainment that can be incorporated into models and used to understand how PDC bulking affects runout. Here we quantify how particle splash, the ejection of particles due to impact by a projectile, entrains particles into dilute PDCs. We use scaled laboratory experiments to measure the mass of sand ejected by impacts of pumice, wood, and nylon spheres. We then derive an expression for particle splash that we validate with our experimental results as well as results from seven other studies. We find that the number of ejected particles scales with the kinetic energy of the impactor and the depth of the crater generated by the impactor. Last, we use a one-dimensional model of a dilute, compressible density current—where runout distance is controlled by air entrainment and particle exchange with the substrate—to examine how particle entrainment by splash affects PDC density and runout. Splash-driven particle entrainment can increase the runout distance of dilute PDCs by an order of magnitude. Furthermore, the temperature of entrained particles greatly affects runout and PDCs that entrain ambient temperature particles runout farther than those that entrain hot particles. Particle entrainment by splash therefore not only increases the runout of dilute PDCs but demonstrates that the temperature and composition of the lower boundary have consequences for PDC density, temperature, runout, hazards and depositional record.

1. Introduction

Pyroclastic density currents (PDCs) are complex multiphase flows governed by mass, momentum, and energy conservation. As a result, any process that adds or subtracts substantial mass, momentum, or energy may be important for PDC dynamics. For example, entrainment of ambient air increases PDC mass, yet its thermal expansion lowers mean PDC density [e.g., *Bursik and Woods*, 1996; *Andrews*, 2014]. When PDC density becomes less than ambient air, the PDC rises buoyantly into the atmosphere—or lifts off. PDC mass, momentum, and energy are also affected by particle exchange with the substrate. For example, sedimentation lowers PDC mass and kinetic and thermal energy [*Freundt*, 1999; *Branney and Kokelaar*, 2002; *Dufek and Bergantz*, 2007], can stop PDC propagation [*Sparks et al.*, 1993; *Dade and Huppert*, 1995; *Dufek*, 2016], and is the process that controls the geologic record of PDCs.

PDCs can also transfer particles from the bed into the current [e.g., *Freundt*, 1999; *Branney and Kokelaar*, 2002]. This process—particle entrainment, the erosion and incorporation of bed material—may also affect PDC dynamics. We currently lack, however, a process-based understanding of "erosion and bulking of currents during transport" that is needed "to simulate the full range of pyroclastic density current behaviors" [*Dufek*, 2016]. While understanding substrate entrainment remains a scientific challenge for geophysical flows [*Iverson and Ouyang*, 2015], erosion by PDCs is well documented through observations of depositional unconformities [*Valentine and Giannetti*, 1995; *Dellino and La Volpe*, 2000; *Branney and Kokelaar*, 2002; *Scarpati and Perrotta*, 2012; *Brand et al.*, 2014], erosional furrows [*Kieffer and Sturtevant*, 1988; *Sparks et al.*, 1997], the removal of scree or topsoil [*Sparks et al.*, 1997; *Cole et al.*, 1998; *Charbonnier and Gertisser*, 2008; *Scarpati and Perrotta*, 2012], lithics and transported blocks within ignimbrites [*Suzuki-Kamata*, 1988; *Buesch*, 1992; *Sparks et al.*, 1997; *Calder et al.*, 2000; *Brand et al.*, 2014; *Roche et al.*, 2016; *Pollock et al.*, 2016], striations against bedrock [*Sparks et al.*, 1997; *Charbonnier and Gertisser*, 2008], and the creation or deepening of channels and gullies [*Cole et al.*, 1998; *Brand et al.*, 2014].

©2016. American Geophysical Union. All Rights Reserved.

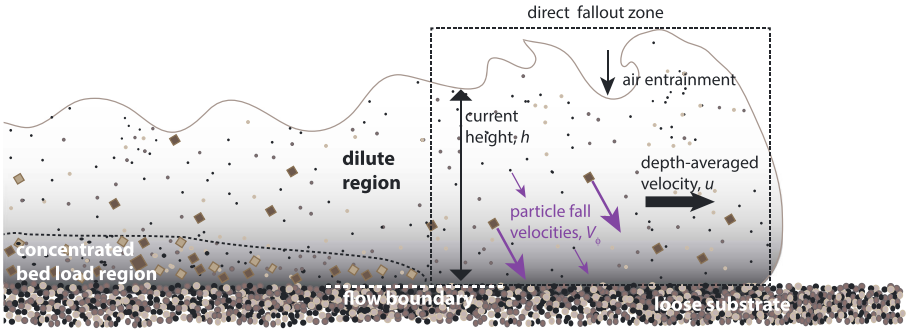

Figure 1. Conceptual model of a pyroclastic density current that can entrain loose substrate particles by particle splash. We hypothesize that splash-driven entrainment occurs in dilute regions of the current where the lower boundary of the flow lacks a bed load region and is dominated by particle fallout.

Recent progress has been made toward connecting observations of erosion with a mechanistic understanding of entrainment processes. These studies have focussed on granular flows and the dense PDC end-member [*Roche et al.*, 2013a; *Roche*, 2015]. Yet the processes that occur at the base of dilute PDCs (e.g., particle rebound and steam generation) are also known to greatly affect PDC dynamics [*Dufek and Bergantz*, 2007; *Dufek et al.*, 2009]. We therefore turn to the dilute PDC end-member and ask (1) How can we mechanistically quantify entrainment? (2) How does particle entrainment affect PDC runout distance? and (3) What entrainment and resuspension processes are important in dilute PDCs?

The lower boundary of dilute PDCs is often conceptualized as a direct fallout zone where sedimenting particles fall onto the underlying substrate or dense undercurrent [e.g., *Branney and Kokelaar*, 2002]. In this setting, we hypothesize that the impact of falling particles against the lower boundary can eject other particles into the current. We test this idea with laboratory experiments and validate an expression for impact-driven particle entrainment. We then use a 1-D model of a dilute PDC to explore how particle entrainment—as parameterized by an expression for particle "splash"—affects dilute PDC density, temperature, and runout distance. We find that particle entrainment can significantly increase PDC runout distance.

2. Conceptual Model of Dilute Pyroclastic Density Currents

Pyroclastic density currents are hot and turbulent mixtures of rock and gas that propagate because of their density difference with air. There are two common end-member models for PDCs (Figure 1): (1) concentrated currents where friction dominates; and (2) dilute currents where there are few particle-particle interactions [e.g., *Branney and Kokelaar*, 2002; *Dufek*, 2016]. Here we study particle entrainment processes relevant to the dilute end-member where individual particles settle through the current and onto the base of the flow (Figure 1). Furthermore, we model the flow boundary as a direct fallout zone where there is a sharp velocity, rheological, and particle concentration gradient between the flow and substrate surface [*Branney and Kokelaar*, 2002]. Our conceptual model, and later our numerical model, therefore requires that dense bed load regions are absent. Because concentrated bed load regions often lag behind the dilute head [*Benage et al.*, 2016], this assumption applies best at the front of PDCs (Figure 1) where the majority of entrainment occurs for at least some flows [*Pollock et al.*, 2016].

PDCs can pass over many different types of surfaces such as rock, water, recent PDC deposits, soil, or vegetation. The composition of this substrate will determine which processes occur at the lower PDC boundary and can thereby affect large-scale PDC dynamics. For example, *Dufek et al.* [2007] quantified the amount of steam generated by pyroclasts as PDCs flow over water and found that steam generation can initiate littoral blasts. *Dufek et al.* [2009] compared two types of PDC boundaries—one that falling particles pass through and one that particles rebound from—and found that particle rebound increased small particle concentration and the transport distance of large clasts.

We consider the case where a dilute PDC passes over loose, unconsolidated soil or PDC deposit (Figure 1). Because active volcanoes can generate multiple PDCs on the decadal timescale, PDCs commonly pass over ash and lapilli. When particles within dilute PDCs hit loose substrate, we hypothesize that the particle impacts can eject substrate particles into the current. In the next section we quantify this process at the particle scale and later introduce particle entrainment into a one-dimensional PDC model.

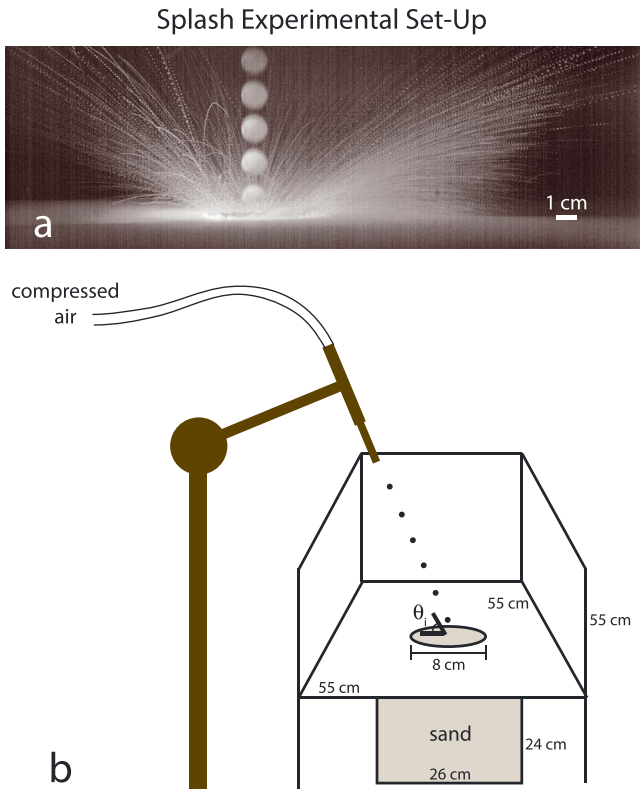

Figure 2. (a) A composite image (100 frames recorded at 600 fps) of a nylon sphere impacting sand and the resultant particle splash. (b) A schematic diagram of our experimental setup. The diameter of the hole in the stiff paper is 8 cm. The high-speed camera was in the foreground.

3. Particle Splash Experiments

Impact-driven particle entrainment, or splash, refers to the ejection of unconsolidated particles from a surface because of impact by a projectile (Figure 2a). While we hypothesize that splash is important within dilute PDCs, this process has been studied in other contexts—particularly with respect to aeolian transport [e.g., *Ungar and Haff*, 1987; *Anderson*, 1987; *Werner*, 1990; *Kok et al.*, 2012]. Splash Functions are mathematical expressions that describe this process, and many empirical, theoretical, and numerical studies have been undertaken to derive and validate Splash Functions (Appendix A). In general, these studies agree that $N_e \propto V_i^n$, where N_e is the number of ejected particles, V_i is the impactor velocity, and n is a coefficient that is typically about 2, consistent with ejection scaling with kinetic energy.

3.1. Experimental and Splash Function scaling

In the next section we present splash experiments with velocities and particle sizes relevant to dilute PDCs. These experiments will allow us to validate a new Splash Function, an expression of the scaling between ejected particle mass and impactor and substrate properties, across this PDC appropriate parameter space. Specifically, we will measure the mass of sand ejected by pumice lapilli impacts. We choose loose, dry sand because of its similarity (size, packing, and texture) to pyroclastic surge deposits [e.g., *Druitt et al.*, 2002; *Burgisser et al.*, 2005] and tendency to settle quickly. We choose pumice lapilli as a direct analog to falling pyroclasts in dilute PDCs.

Previous studies have conducted splash experiments with 0.2–20 mm diameter particles, 0.25–60 m s^{-1} velocities, and impacting and ejected particles with the same diameters (Table 1). We will also test our Splash Function with data from these seven studies. As long as the same processes (e.g., transfer of kinetic to potential energy) control particle splash, our Splash Function, if valid, should apply to this extended parameter range. We note, however, that no experiments have measured particle splash when a small particle impacts a bed of larger particles. Any Splash Function extrapolation to this scenario, or far beyond the parameter space shown in Table (1), is therefore unvalidated.

Table 1. Splash Function Study Comparison

Study	Method	Impactor Type and Diameter	Substrate Type and Diameter	Impactor Velocity ($m\ s^{-1}$)	$\frac{m_i}{m_e}$	$\frac{\rho_i}{\rho_e}$	N[a]
Mitha et al. [1986]	experiments	4 mm steel BBs	4 mm steel BBs	21–25	1	1	1
Willetts and Rice [1986]	experiments	0.2–0.5 mm sand	0.2–0.5 mm sand	3–4	1	1	≈ 100
Werner and Haff [1986]	2-D simulations	10; 20 mm	20 mm	30–81	0.25; 1	1	60
Anderson and Haff [1988]	2-D simulations	1 mm	1 mm	0.25–8	1	1	≈ 10
Beladjine et al. [2007]	experiments	6 mm PVC plastic	6 mm PVC plastic	18–39	1	1	100
Oger et al. [2008]	2-D and 3-D simulations	6 mm	6 mm	30–60	1	1	≈ 40
Wu [2013]	3-D simulations	0.3 mm	0.3 mm	4–10	1	1	≥ 1
This study	experiments	11 mm pumice, 12 mm wood, 13 mm nylon	0.56 mm sand	5–65	3600–5000	0.33–0.47	1

[a] N is the number of experiments for a given set of input parameters.

3.2. Experimental Methods

We used laboratory experiments to measure the mass of sand ejected during impact by a projectile. To create impacts, we propelled 1.2 cm diameter particles with compressed air into dry sand. In these experiments we varied impactor type (natural pumice clasts, nylon spheres, and wood spheres) and density (0.88–1.25 g cm^{-3}), impactor speed (5–65 m s^{-1}), and impact angle (40–90°). We conducted sixty-one experiments in which did not vary the type of material in the substrate (0.56 mm diameter loosely packed sand).

During the experiments we measured the impactor velocity immediately prior to impact with a high-speed camera at 1000 frames per second (fps). We estimated the uncertainty of the velocity measurements to be 2 pixels/frame × 1000 fps × 1 cm/20 pixels = 1 m s^{-1} [*Birch et al.*, 2014]. We set the impact angle by rotating the arm of the compressed air blaster (Figure 2b). A 26 × 26 × 24 cm container (large enough to avoid edge effects) held the sand, and we stirred the sand such that it was loosely packed before each experiment. To measure the total mass of suspended particles, we placed stiff paper 1 mm above the sand surface. The paper contained an 8 cm diameter hole to allow for particle escape; we fired the projectile into the center of this hole such that the majority of suspended material landed on the paper (Figure 2). Vertical walls blocked high-velocity ejected particles from traveling off the edge of the collection paper (Figure 2). After each experiment, we collected and weighed the sand. If the projectile rebounded upon impact, the rebound velocity was measured with the high-speed camera. As did *Dufek et al.* [2009], we found that the impactor rebounded more often at shallow incidence angles, θ_i, and only when $\theta_i \leq 70°$. Rebound occurred during relatively few experiments.

Our methods for measuring suspended particle mass underestimated suspended mass for several reasons. First, suspended particles that landed within the 8 cm diameter hole were not collected. Furthermore, particles that would have been ejected from locations outside the hole opening were not able to escape. Lastly, particles that were ejected toward the camera were not caught on the paper.

3.3. Experimental Results

Figure 3 shows experimental measurements of the ratio of ejected to projectile mass versus a dimensionless ratio of kinetic to potential energy. We found that the total suspended mass increased with the square of the impact velocity and that the ejected mass generally exceeded the mass of the impactor. Pumice (0.99 and 1.25 g cm^{-3}) ejected, in general, more particles than the wood spheres (0.88 g cm^{-3}) of similar impact speeds. We hypothesize that this is because pumice has a rough and irregular surface that can grab and eject more sand than smoother spheres.

We compare our experimental results to several previously published Splash Functions in Appendix A. The fits to all these functions are unsatisfactory (Figures A1a–A1f). Many of the existing expressions are off by several orders of magnitude. We also test our experimental results against Splash Functions where $N_e \propto (V_i \sin\theta_i)^2$ and $N_e \propto V_i^2$, where θ_i is the incidence angle of the impactor (Appendix B). Appendix B shows that we find better fits when V_i is used instead of $V_i \sin\theta_i$. In the next section we derive a new Splash Function that we compare to our experimental results as well as measurements from seven other studies.

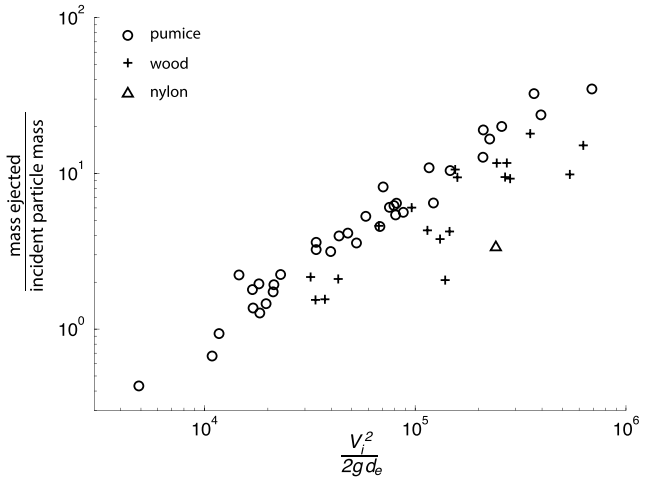

Figure 3. Experimental measurements of ejected mass over the mass of the incident particle, m_i, plotted against a dimensionless ratio of kinetic to potential energy. Our experimental results demonstrate that $\frac{N_e m_e}{m_i}$ increases with V_i^2 and that impacts can suspend masses greater than the incident particle mass (i.e., $\frac{N_e m_e}{m_i} > 1$). Wood spheres eject less mass than pumice for a given kinetic energy.

4. Splash Function

We derive a new Splash Function based on a conversion of kinetic energy to potential energy. While other Splash Functions have been derived based on energy conservation [e.g., *Mitha et al.*, 1986; *Ungar and Haff*, 1987; *Andreotti*, 2004; *Wu*, 2013], we allow impacting and ejected particles to have different sizes and densities.

Consider an impacting particle with kinetic energy $\frac{1}{2} m_i V_i^2$, where m_i is the mass of the impactor, and V_i is the impactor velocity. During a collision the kinetic energy of the impacting particle (1) contributes to the plastic and elastic deformation of both the impactor and the substrate, (2) is dissipated by friction in between substrate particles, (3) is retained by the impacting particle and results in particle rebound, and (4) is transferred to the substrate and results in particle ejection. We write the conversion of kinetic energy of the impactor to potential energy of the substrate as

$$e_n^2 \frac{1}{2} m_i V_i^2 = N_e m_e g L \,, \tag{1}$$

where $0 < e_n < 1$ is a restitution coefficient that characterizes the kinetic energy fraction transferred to the ejected particles (energy lost from processes 1–3), m_e is the mass of each ejected particle, g is gravity, L is a characteristic length scale of suspension, and N_e is the number of ejected particles.

The diameter of the ejected particles, d_e, has been used as the characteristic length scale in other Splash Functions [*Mitha et al.*, 1986; *Anderson*, 1987; *Andreotti*, 2004; *Wu*, 2013]. However, *Oger et al.* [2008] demonstrated that the number of suspended particles does not scale linearly with V_i^2. We propose that the relevant length scale for particle suspension is the depth of the crater that is formed during impact. While there are many expressions for crater depth in dry granular media we use

$$d_c = 0.14 \mu^{-1} \sqrt{\frac{\rho_i}{\rho_e}} d_i^{\frac{2}{3}} h_i^{\frac{1}{3}} \,, \tag{2}$$

where μ is the tangent of the friction angle, ρ_i is the impactor density, ρ_e is the ejected particle density, d_i is the impactor diameter, and h_i is the height from which the impactor is dropped [*Newhall and Durian*, 2003]. h_i can be related to V_i according to $h_i = \frac{V_i^2}{2g}$. We thereby propose a new Splash Function,

$$N_e = \frac{\frac{1}{2} e_n^2 m_i V_i^2}{0.14 m_e g \mu^{-1} \sqrt{\frac{\rho_i}{\rho_e}} d_i^{\frac{2}{3}} \left(\frac{V_i^2}{2g}\right)^{\frac{1}{3}}} \,, \tag{3}$$

where $N_e \propto V_i^{\frac{4}{3}}$.

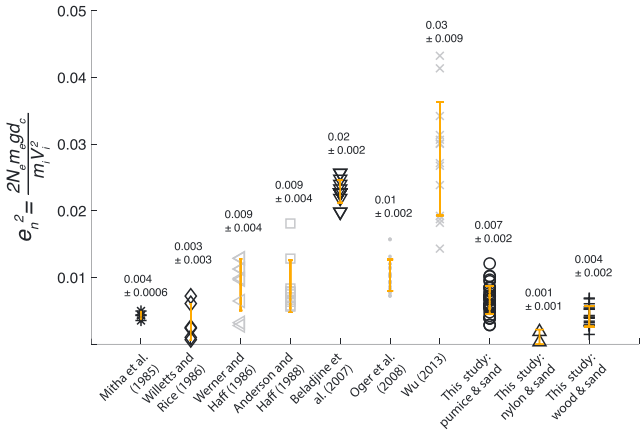

Figure 4. Measurements of particle splash from eight studies are plotted to solve for a mean restitution coefficient, e_n^2, which represents the fraction of energy retained during impact. The orange bars show the mean and standard deviation of the restitution coefficient for each study. For most studies, restitution coefficients fall within a small range. This demonstrates that the restitution coefficient is fairly constant for the range of materials, impact velocities, and angles used in each study. It is not surprising that e_n^2 varies between studies because different materials were used. Black symbols represent data from physical experiments, and gray symbols represent data from discrete element model (DEM) simulations.

4.1. Splash Function Validation

We test equation (3) by comparing N_e predicted to N_e observed. To do this, we use our experimental measurements as well as measurements from seven other studies (Table 1) [*Mitha et al.*, 1986; *Willetts and Rice*, 1986; *Werner and Haff*, 1986; *Anderson and Haff*, 1988; *Beladjine et al.*, 2007; *Oger et al.*, 2008; *Wu*, 2013]. These studies allow us to validate our Splash Function against impactor velocities of 0.25–65 m s^{-1}, particle sizes of 0.2–20 mm, and impactor to substrate mass ratios of 1–5000 (Table 1).

Because each study used different physical materials or numerical parameters, we expect e_n^2 in equation (3) to be different for each study. We solve for e_n^2 by rearranging equation (3) and using values reported by each study for $\frac{m_i}{m_e}$, V_i, $\frac{\rho_i}{\rho_e}$, d_i, and N_e; we assume $\mu = 0.5$. If equation (3) is valid, e_n^2 should have a relatively constant

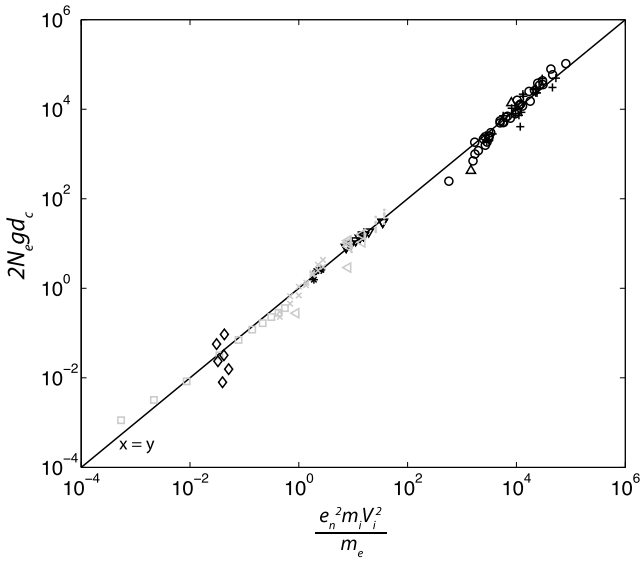

Figure 5. Equation (3) is tested by substituting measured values from eight studies into equation (3). Equation (3) holds (plots on a 1:1 line) across a large parameter space ($0.25 < V_i < 81$ m s^{-1} and $0.02 < d_i < 2$ cm), suggesting that equation (3) is a valid Splash Function. Black symbols represent data from physical experiments, and gray symbols represent DEM simulations. The symbol shapes correspond to those in Figure 4.

value for each study. Figure 4 shows that each study reports a different restitution coefficient that, with the exception of *Wu* [2013], has small standard deviations. This suggests that equation (3) fits the experimental data well.

We rearrange equation (3) and plot $\frac{e_n^2 m_i V_i^2}{m_e}$ versus $2gN_e d_c$, using the e_n^2 values given in Figure 4 and where the other parameters were reported by each study (Figure 5). Figure 5 shows that equation (3) matches observations of particle splash across a wide parameter range. Because fall velocities and particle sizes in dilute PDCs are generally within the parameter range for which equation (3) was validated, we feel confident that equation (3) can be used in models of particle settling in dilute PDCs where the ejected particle is no larger than the impactor.

5. One-Dimensional Model of a Dilute Pyroclastic Density Current That Entrains Air and Sediment

We examine PDC runout distance in a 1-D model of a dilute (no frictional deceleration) and turbulent gravity current across a flat surface. A feature of this model is that we allow the fluid (air) in the PDC to be compressible such that thermal expansion of entrained air can change current density. We also model the effects of particle sedimentation and entrainment on PDC density. PDC density is critical to this model because we define runout distance as the location where the bulk current density is equal to the density of ambient air; this is where liftoff occurs. All quantities vary as a function of distance, x, traveled or equivalently as time, t. We do not explicitly highlight the spatial and temporal variability of the variables in the equations that follow.

Consider a dilute pyroclastic density current with three phases: an air phase with mass per unit area m_a (kg m^{-2}), a small particle phase with mass per unit area m_{ϕ_1} (kg m^{-2}), and a large particle phase with mass per unit area m_{ϕ_2} (kg m^{-2}). Here mass, and later energy, are divided by the local basal area of the current; thus, m is a bulk density multiplied by the current thickness. Let the initial temperature of the particles be T_i and the initial temperature of air entrained into the current be the ambient temperature T_a. Energy transfer between particles and air in the current is rapid [*Stroberg et al.*, 2010] such that the entrained air is heated and the mean temperature of the PDC is

$$T_c = \frac{H}{C_p^a m_a + C_p^r (m_{\phi_1} + m_{\phi_2})}, \tag{4}$$

where C_p^a and C_p^r are the specific heat capacities of air and rock, respectively (J kg^{-1} K^{-1}), and H is the thermal energy in the current per unit area (J m^{-2}),

$$H = C_p^a T_a m_a + C_p^r T_i (m_{\phi_1} + m_{\phi_2}). \tag{5}$$

The height of the current, h, depends on the volume of air and particles in the current. We let air volume change due to thermal effects such that

$$h = \frac{m_a}{M}\frac{RT_c}{P} + \frac{m_{\phi_1}}{\rho_{\phi_1}} + \frac{m_{\phi_2}}{\rho_{\phi_2}}, \tag{6}$$

where M is the molar mass of air (kg mol^{-1}), R is the universal gas constant (J mol^{-1} K^{-1}), P is pressure within the current (Pa), and ρ_{ϕ_1} and ρ_{ϕ_2} are the densities of the two particle size fractions (kg m^{-3}). Because the PDC is denser than the air in which it propagates, the pressure within the current will be slightly higher than atmospheric. In the model, however, we assume that P is atmospheric pressure. The bulk density of the density current is thus

$$\rho_c = \frac{m_a + m_{\phi_1} + m_{\phi_2}}{h}. \tag{7}$$

We can now solve equations for conservation of mass, momentum, and energy in a current that entrains air, sediments particles, and entrains particles. Because turbulent gravity current motion across a flat surface is governed by a pressure gradient at the head of the current, momentum conservation can be written as [e.g., *Dade and Huppert*, 1995; *Roche et al.*, 2013b]

$$u = \mathrm{Fr}\sqrt{g'h}, \tag{8}$$

where Fr is a Froude number ($Fr = \sqrt{2}$ when there is no energy loss), $g' = \frac{\rho_c - \rho_a}{\rho_a} g$, u is the depth-averaged current velocity in the downstream direction, g is gravity, and h is the height of the current. Because fluid

resistance causes energy loss, observed density current Froude numbers are generally slightly lower than $\sqrt{2}$, and we use $Fr = 1.2$ [*Huppert and Simpson*, 1980].

Mass within the current changes due to air entrainment, particle sedimentation, and particle entrainment. We write separate continuity equations for the air and particle fractions of the current. The continuity equation for air is

$$\frac{dm_a}{dt} = Eu\rho_a, \tag{9}$$

where E is the entrainment rate of air into the current and ρ_a is the density of air at T_a. The right-hand side of equation (9) dictates that the mass of air in a PDC changes due to air entrainment where the velocity of air entering the current normal to the entraining edge is Eu. The continuity equations for the two particle size fractions are

$$\frac{dm_{\phi_1}}{dt} = \underbrace{\frac{-m_{\phi_1}V_{\phi_1}}{h}}_{\text{settling}} + \underbrace{\beta V_{\phi_1}^{4/3}}_{\text{splash from } m_{\phi_1}} + \underbrace{\beta V_{\phi_2}^{4/3}}_{\text{splash from } m_{\phi_2}}, \tag{10}$$

$$\frac{dm_{\phi_2}}{dt} = \underbrace{\frac{-m_{\phi_2}V_{\phi_2}}{h}}_{\text{settling}}, \tag{11}$$

where V_{ϕ_1} and V_{ϕ_2} are the settling velocities of the two particle size fractions, $\beta = \frac{\frac{1}{2}e_n^2 m_i}{0.14 g\mu^{-1}\sqrt{\frac{\rho_i}{\rho_e}}\left(\frac{d_J^2}{2g}\right)^{\frac{1}{3}}}$ is a coefficient given by our Splash Function, equation (3), and m_i is the total mass of the impactors, $\int \frac{m_\phi V_\phi}{h} dt$, for particle size fractions ϕ_1 and ϕ_2. The second and third expressions on the right-hand side of equation (10) show that we assume that the entrained particles have the same physical properties (size and density) as the small particle fraction. Furthermore, we assume that the settling particles are traveling at their terminal velocities when they settle from the current. We calculate settling velocities according to the framework presented by *Dufek et al.* [2009]; see also Appendix C.

Thermal energy within the current changes due to entrainment of air, entrainment of particles, and sedimentation of particles. We neglect the conversion of gravitational potential to heat and dissipation of kinetic energy to heat. We write conservation of thermal energy as

$$\frac{dH}{dt} = \underbrace{\frac{dm_a}{dt}C_p^a T_a}_{\text{air entrainment}} - \underbrace{\left(\frac{m_{\phi_2}V_{\phi_2}}{h} + \frac{m_{\phi_1}V_{\phi_1}}{h}\right)C_p^r T_c}_{\text{settling}} + \underbrace{\left(\beta V_{\phi_1}^{4/3} + \beta V_{\phi_2}^{4/3}\right)C_p^r T_e}_{\text{splash}}, \tag{12}$$

where T_e is the temperature of the particles entrained into the current. The first term on the right-hand side of equation (12) represents entrainment of ambient air into the current, the second term on the right-hand side accounts for particle sedimentation, and the third term accounts for particle entrainment.

Equations (4)–(12) allow us determine the time, t_r, at which $\frac{\rho_c}{\rho_a} \leq 1$. Because $u = \frac{dx}{dt}$, runout distance L_r is

$$L_r = \int_{t_o}^{t_r} u dt. \tag{13}$$

We use a first-order, forward-difference scheme to solve equations (4)–(13) and determine runout distances for thermally expanding currents, noting that all quantities (m_a, m_{ϕ_1}, m_{ϕ_2}, T_c, H, h, ρ_c, u, V_{ϕ_1}, and V_{ϕ_2}) are functions of x and equivalently t. We compare runout distances for currents that do not sediment particles, sediment but do not entrain, and entrain particles according to equation (3). Furthermore, we vary the temperature of entrained particles, T_e.

5.1. One-Dimensional PDC Model Results

We use the 1-D model to explore how particle entrainment by splashing can affect PDC dynamics and runout distance. Figure 6 shows how density and temperature evolve in PDCs with different degrees of particle sedimentation and particle entrainment. For all model results plotted in Figure 6, $T_a = 20°C$, $T_i = 600°C$, and the

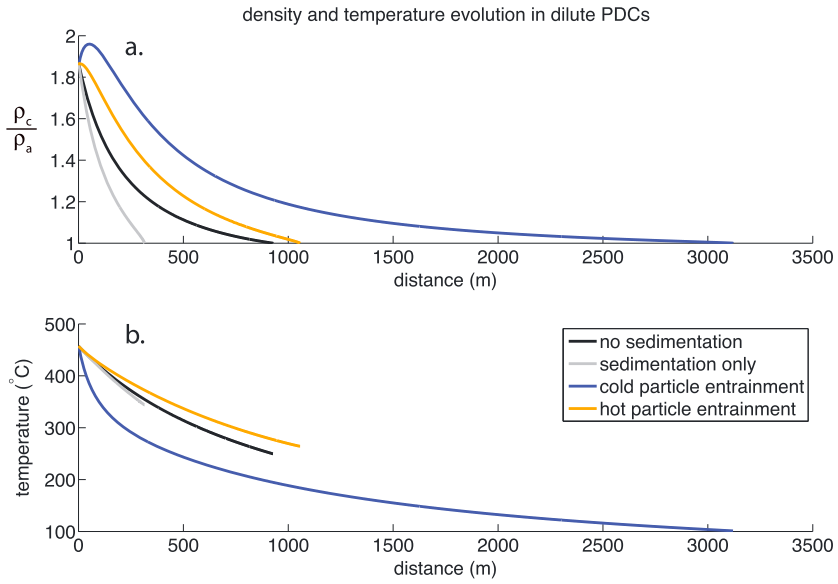

Figure 6. (a) Density and (b) temperature model results as a function of distance within currents with four different particle sedimentation and entrainment regimes. All currents had an initial particle temperature of 600°C and initial mean PDC temperature of 457°C . The PDC that entrains cold particles runs out the farthest and has the highest mean density and lowest internal temperature. The PDC that entrains hot particles runs out the second farthest and has the second highest mean density but maintains the highest internal temperature.

initial values for m_a, m_{ϕ_1}, and m_{ϕ_2} are 30, 100, and 10 kg m^{-2}, respectively. The diameters and densities of the small and large particles are 0.1 and 10 mm and 2400 and 1000 kg m^3, respectively. We choose a small diameter for the small particle size fraction such that particles ejected into the current by splash can be assumed to be mixed within the current by turbulence. While particle settling velocities evolve as a function of PDC density and particle concentration (Appendix C), the initial settling velocities for these two particle size fractions were 0.5 and 8.7 m s^{-1}, respectively. We let $E = 0.1$ [*Andrews*, 2014] and the splash restitution coefficient equal the value we empirically determined for pumice impacting sand, $e_n^2 = 0.007$ (Figure 4). Cold particle entrainment refers to a PDC that entrains particles at temperature T_a, while hot particle entrainment refers to entrainment of particles at the initial PDC mixture temperature.

Figure 6a shows how PDC densities evolve with distance. Density increases over a distance of 0 to 49 m for the current that entrains cold particles. Otherwise, density decreases with distance for all the currents. The PDC that entrains cold particles has the highest density, followed by the current that entrains hot particles. This shows that particle splash can keep PDC density elevated. Runout is shortest, and the density declines the steepest, for the current that sediments but does not entrain particles.

PDC mean temperature is plotted with distance in Figure 6b. Internal PDC temperature declines most rapidly for the PDC entraining cold particles. By comparison, PDC temperature remains the highest for the current entraining hot particles.

We examine the effects of entrainment on PDC runout distance over a range of initial mean PDC temperatures (Figure 7). Except for initial temperature (and therefore initial settling velocity), the parameters used in Figure 7 were the same as those listed for Figure 6. Runout distance is defined as the location where $\frac{\rho_c}{\rho_a} \leq 1$. Figure 7 shows that runout distance decreases with increasing initial PDC temperature. PDCs that do not sediment or entrain particles show the steepest decline in runout with temperature. This is because these currents have only one mechanism to lower density—the thermal expansion of entrained air, which is highly effective at high temperatures and less effective at low temperatures. By comparison, the sedimenting and sediment entraining currents can change density through particle exchange with the substrate.

It is useful to compare PDCs that entrain particles to PDCs that sediment but do not entrain. Figure 7 shows that PDCs that entrain cold particles run out almost an order of magnitude farther than PDCs that entrain hot particles, which run out a half an order of magnitude farther than PDCs that sediment only (Figure 7). This demonstrates that particle splash can be important for PDC runout distance and dynamics.

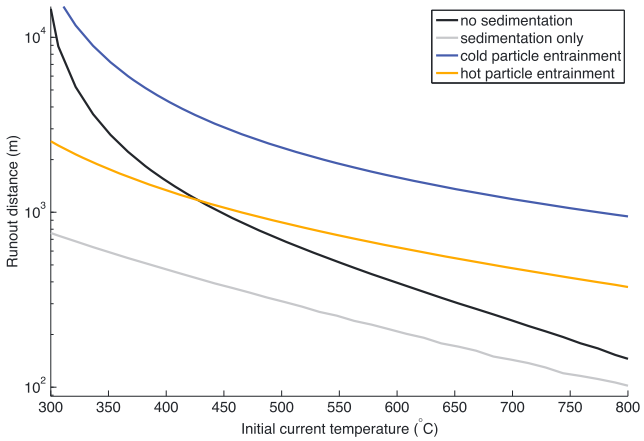

Figure 7. Runout distance model results. Runout decreases with initial temperature for all currents. The occurrence and temperature of particle entrainment have order of magnitude effects on runout distance. PDCs that entrain cold particles run out the farthest.

Furthermore, the importance of sedimentation regime decreases with initial PDC temperature as thermal expansion becomes more important than sedimentation at high PDC initial temperatures.

6. Discussion

In section 1 we highlighted three questions. We now address these in order, in light of our experiments and model results.

6.1. Quantification of Particle Entrainment

We quantified particle entrainment with a new Splash Function and found that the number of ejected particles scales with impact crater depth, equation (3). Unlike existing Splash Functions, we considered physical differences between the impactor and the ejected particles. We also demonstrated that our Splash Function applies across a broad parameter space and can describe the dynamics of sand or lapilli pumice impactors. Overall, splash can result in the net addition of particles to PDCs because the ejected mass can be greater than the projectile mass (Figure 3). In our model we assumed that splashed particles were fully mixed within the PDC and did not explicitly account for the splashed particle momentum flux. Three-dimensional multiphase models, however, could in principle consider the velocity distributions of ejected particles [e.g., *Kok et al.*, 2012].

6.2. The Effect of Particle Entrainment on PDC Runout Distance

We used a 1-D model to test the effects of particle splash on dilute PDC runout distance. We defined runout distance as the location where $\frac{\rho_c}{\rho_a} \leq 1$ and found that particle entrainment can increase runout by over an order of magnitude (Figure 7). This result implies that the composition of the lower boundary of a PDC can have an important influence on runout distance. Where loose particles are available for splash, such as on a previous PDC deposit, PDCs may run out much farther because particle entrainment increases flow density. By comparison, if a particle source is not available — where the terrain is bedrock, water, or covered by vegetation — then splash-driven particle entrainment is unlikely to occur and runout distances may be shorter.

The temperature of the entrained particles also greatly affects PDC runout distance and density evolution. This is because hot particles add more thermal energy to the flow and lower air density. Our results agree with those of *Freundt* [1999] and imply that a dilute PDC overriding a hot substrate (such as a recent ignimbrite deposit) will not run out as far as one overriding a cold deposit.

We examined the effects of particle splash in the absence of a concentrated bed load region. It is possible, however, that dense basal layers of PDCs may inhibit particle splash by slowing falling particles and buffering the substrate. Indeed, entrainment mechanisms other than particle splash are likely important in the bed load region [*Roche et al.*, 2013a; *Roche*, 2015].

Particle splash may, however, provide a mechanism through which mass and momentum are exchanged between the dense and dilute regions of a PDC. While mobile bed loads are fundamentally different from

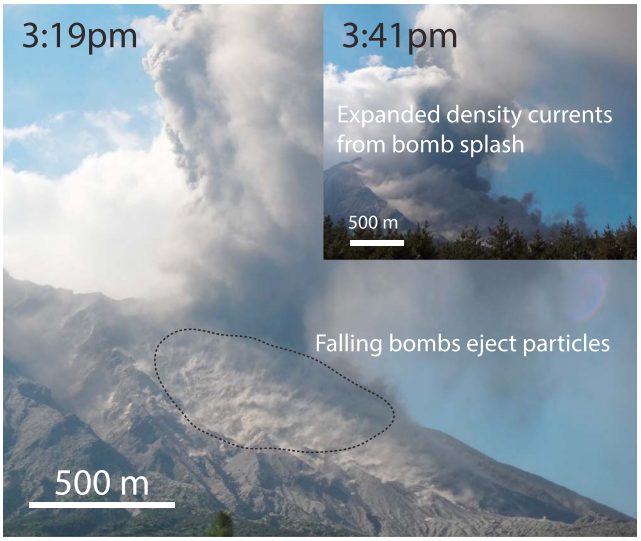

Figure 8. The impact of bombs on the flank of Sakurajima volcano, Japan, on 22 July 2013 generates small density currents during a Vulcanian eruption.

static and concentrated granular substrates, we envisage that particles falling from the dilute region of a PDC onto a concentrated bed load region may be able to splash particles from the bed load into the dilute part of a PDC. If splash on a granular flow is as efficient as splash on a static granular layer, then dilute PDCs overriding a hot and dense flow will have shorter runout distances than those on cold and static granular substrates (Figure 7).

The initial temperature of a PDC can greatly affect runout distance (Figure 6) and air entrainment efficiency [*Benage*, 2015]. Air entrainment during collapse events has been invoked as the mechanism that cools PDCs to temperatures less than magmatic [e.g., *Sparks et al.*, 1978]. Particle splash may be an additional mechanism for PDC cooling during or soon after PDC formation (Figure 6b). For that reason, models of PDC formation via collapse [e.g., *Neri et al.*, 2003] could examine how particle splash affects initial PDC temperature. Equally important, splash-driven entrainment can be incorporated into 3-D multiphase and multiphysics PDC simulations [e.g., *Todesco et al.*, 2002; *Dufek and Bergantz*, 2007; *Doronzo et al.*, 2010; *Esposti-Ongaro et al.*, 2012; *Benage et al.*, 2016] to test how entrainment affects not only runout but concentration and concentration gradients, stratification, air entrainment, and thermal evolution within the flows. Three-dimensional multiphase models can also explore how particle splash modifies the momentum flux into the currents and examine how high bed load concentrations [e.g., *Andrews and Manga*, 2012; *Dufek et al.*, 2015] affect the occurrence and efficiency of particle splash.

It would be interesting and informative to know how much of a PDC is composed of primary versus entrained material. We do not report this kind of information in part because differentiating juvenile from entrained material is complex. Entrained particles can be lithics, part of older deposits, or can be sourced from recently deposited parts of the PDC itself. Individual particles may go through many cycles of deposition and resuspension before reaching their final fates in coignimbrite plumes or ignimbrite deposits.

6.3. Entrainment Processes in Dilute PDCs

Here we have proposed that splash can drive particle entrainment in dilute PDCs. Indeed, particle saltation has been observed in large-scale physical models of dilute PDCs [*Lube et al.*, 2015] and proposed as a mechanism to suspend particles in dilute PDCs [*Denlinger*, 1987]. *Valentine and Giannetti* [1995] observed a pyroclastic surge deposit containing a layer of well-sorted angular pumice clasts and proposed that plinian fallout through a pyroclastic surge emplaced this layer and created a "locally gradational or erosional" boundary between the surge and fallout deposit. We hypothesize that the unconformity between the surge and fallout deposit may be, at least partially, due to erosion by particle splash.

Alternatively, shear and the mobilization of particles by fluid drag may also drive particle entrainment in PDCs as it does in rivers and turbidity currents [e.g., *Garcia and Parker*, 1993; *Dufek et al.*, 2015; *Roche*, 2015]. Splash, however, dominates entrainment in flows where viscosity and density are low and gravity is high such as for

windblown particle transport on Earth and Mars [*Werner*, 1990; *Andreotti*, 2004; *Kok et al.*, 2012]. Because dilute PDCs are also dilute air-particle mixtures and experiments have shown that splash can suspend particles of equal and lesser size than the impactor, it is likely that splash also dominates entrainment in these flows. Future work can (1) look for evidence for splash in PDC models and deposits and (2) use experimental, theoretical, and numerical techniques from the aeolian transport literature [*Durán et al.*, 2011; *Kok et al.*, 2012] to compare the magnitudes of shear and splash-driven entrainment in PDCs.

Particle splash may not just be a mechanism for particle entrainment but also for PDC generation [e.g., *Branney and Brown*, 2011]. Bomb impacts may create small density currents, and during a 22 July 2013 vulcanian eruption from Showa crater, Sakurajima volcano, Japan, we observed particulate clouds and density currents immediately following the ejection of large bombs onto the flanks of Sakurajima (Figure 8). Our interpretation is that the bomb impacts ejected loose particles that expanded into a particulate cloud and density current. There are, however, alternative explanations for this ash cloud suspension such as its generation through strong ground vibrations caused by the eruption.

7. Conclusions

Pyroclastic density currents can be both erosional and depositional, yet we currently lack quantitative descriptions of erosional mechanisms [e.g., *Branney and Kokelaar*, 2002; *Dufek*, 2016]. In this study, we proposed that impacts from particles falling out of PDCs can eject or "splash" particles back into the currents. We used laboratory experiments to demonstrate that this happens at the particle scale and to measure the number of particles ejected by impacts of pumice, wood, and nylon spheres. We found that the number of ejected particles increases with the kinetic energy of the impactor and developed a new quantitative expression for particle splash based on energy conservation, equation (3). Unlike previously proposed Splash Functions, we found that the appropriate length scale for the suspended particles is the depth of the crater created during an impact.

We incorporated splash and equation (3) into a 1-D model of a dilute, compressible density current to examine the effects of particle entrainment on PDC runout. We found that particle entrainment by splash can increase the runout of PDCs by up to an order of magnitude because entrainment by splash increases current density (Figures 6 and 7). The temperature of the entrained particles also has an important effect on PDC temperature evolution and runout (Figures 6 and 7). Currents that entrain cold particles run out farther than those that entrain hot particles because hot particles add more thermal energy to the flows and lower air density. Our results show that the temperature and composition of the lower boundary of PDCs can greatly influence PDC runout.

While it is difficult to observe splash in natural PDCs, we hypothesize that falling bombs generated the ash clouds observed during a vulcanian eruption at Sakurajima volcano, Japan, and that erosional boundaries observed between fallout and surge deposits are due to particle splash. Future work can use experiments, models, and field observations to verify the occurrence of particle splash in PDCs. Splash Functions allow particle entrainment to be mechanistically incorporated into 3-D multiphase and multiphysics models to determine how entrainment affects PDC concentration, stratification, thermal evolution, air entrainment, and runout.

Appendix A: Splash Function Comparison

Here we briefly present several studies of Splash Functions and compare them to experimental measurements. Table 1 lists the parameter space explored by each study. *Werner* [1990] found that

$$N_e = 3.36(0.00572V_i - 0.915)\sin\theta_i\,, \tag{A1}$$

where N_e is the number of suspended particles, θ_i is the impact angle with respect to horizontal, V_i is the incidence velocity of the impactor, and g is gravity. *Oger et al.* [2008] proposed

$$N_e = 0.55(V_i - 40\sqrt{gd})\,, \tag{A2}$$

and

$$N_e = 0.4(V_i - 4.0) + (V_i - 25)\sin\theta_i\,, \tag{A3}$$

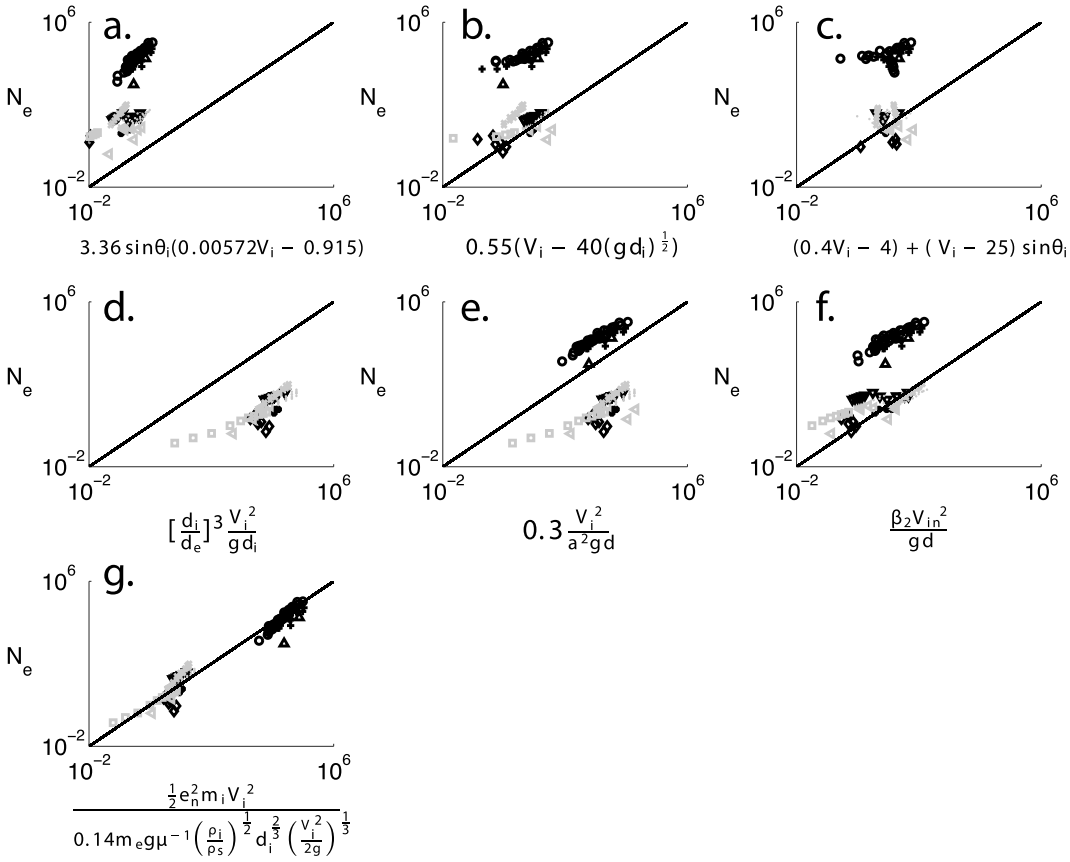

Figure A1. Splash Function predictions versus the observed number of ejected particles from eight studies (Table 1). The symbols correspond to those shown in Figure 4. Gray represents data from numerical studies, and black represents data from physical experiments. Where d was unspecified we let $d = d_i$. (a) *Werner* [1990]; (b and c) *Oger et al.* [2008]; (d) *Anderson* [1987] where $a = 1$; (e) *Andreotti* [2004]; (f) *Wu* [2013] where $e_n^2 = 0.008$ and $\alpha = 1$; and (g) the Splash Function from this study, equation (3), where $e_n^2 = 0.008$ and $\mu = 0.5$. Figure A1g (our Splash Function) shows that predictions match observations.

where d is the diameter of both the impacting and ejected particles. Particle splash has also been described with energy-based models. *Ungar and Haff* [1987] hypothesized that a portion of the kinetic energy of the impacting particle is transferred to the potential energy of the substrate such that $N_e \propto \frac{V_i^2}{gd}$. *Anderson* [1987] extended this analysis and proposed

$$N_e = \left(\frac{d_i}{d_e}\right)^3 \frac{V_i^2}{g d_e}. \tag{A4}$$

Similar energy-based Splash Function models have been suggested by *Andreotti* [2004],

$$N_e = 0.3\frac{V_i^2}{a^2 g d}, \tag{A5}$$

where a is a scaling factor, and *Wu* [2013],

$$N_e = \frac{\beta V_{in}^2}{gd}, \tag{A6}$$

where $\beta = \frac{e_n^2}{2\alpha}$, V_{in} is the normal component of the impactor velocity, e_n is a restitution coefficient, and α is a correction coefficient.

All the expressions suggest that N_e should increase with V_i, and equations (A4)–(A6) suggest $N_e \propto \frac{V_i^2}{gL}$, where L is a length scale. However, only equation (3) considers impactor and bed particles of different sizes. None of these expressions consider differing densities or elastic properties between impactor and bed particles.

Table B1. *p* Value Model Fit Comparisons[a]

	d_c	d_e
V_i	0.91	0.71
V_{in}	0.71	0.58

[a]A combination of d_c and V_i provides the *p* value closest to 1 and the best model fit.

We test equations (A1)–(A6) against our experimental measurements as well as data from seven other studies (Table 1). Figure A1 shows that these existing Splash Functions do not fit the data. By comparison, Figure A1g shows our Splash Function, equation (3), where $e_n^2 = 0.008$ fits the data fairly well.

Appendix B: Alternative Splash Functions

Figure A1 shows that existing Splash Functions are unsatisfactory across a wide parameter range. While section 3 proposed a single new Splash Function, we explore alternative Splash Functions of the form

$$N_e = \frac{e_n^2 \frac{1}{2} m_i V^2}{m_e g L}, \tag{B1}$$

where V can be either the magnitude of velocity, V_i, or the component normal to the bed, V_{in}, and L can be d_e or d_c. To test these alternative Splash Functions, we plot N_e predicted versus N_e observed and fit a log linear line to the trends. Based on data shown in Figure 4, we let e_n be 0.08 for all trials. The slope of the log linear line represents the power law exponent, p, for $N_e^{\text{observed}} \propto \left(N_e \text{calculated}\right)^p$. A p value close to 1 demonstrates a good model fit. Table B1 shows the outcome from these trials. Choosing $V = V_i$ and $L = d_c$, which was presented as equation (3) in the main manuscript, provides the best fit.

Appendix C: Settling Velocities

We calculate settling velocities using the formulation in *Dufek et al.* [2009]. The change in settling velocity, V, of a particle is

$$\frac{dV}{dt} = F_g + F_s + g\left(\frac{2\rho_p - \rho_g}{2\rho_p + \rho_g}\right), \tag{C1}$$

where F_g is the force of gas on the particles, F_s is the force of many small particles on larger particles, ρ_p is the particle density, and ρ_g is the gas density. F_g is described through a drag term that is a function of the particle Reynolds number,

$$\text{Re}_\text{p} = \rho_g \frac{Vd}{\mu_g}, \tag{C2}$$

where μ_g is the dynamic viscosity of the gas and d is the particle diameter. The force of gas against a particle is

$$F_g = \frac{fV}{\tau_p}\left(\frac{2\rho_p}{2\rho_p + \rho_g}\right), \tag{C3}$$

where f if is an empirical correction to the drag coefficient,

$$f = 1 + 0.15\,\text{Re}_\text{p}^{0.687} + \frac{0.0175}{1 + 42500\,\text{Re}_\text{p}^{-1.16}}, \tag{C4}$$

and τ_p is the particle response time,

$$\tau_p = \frac{(\rho_p - \rho_g)d^2}{18\mu_g}. \tag{C5}$$

F_s is the force imparted on large particles by small particles.

$$F_s = \left(\frac{6\alpha_{\phi_1}\sqrt{\theta}g_o(d_{\phi_1} + d_{\phi_2})^2}{\sqrt{\pi}d_{\phi_1}^3}\right)\left(\frac{\rho_1 d_{\phi_1}^3(1+e)(V_{\phi_1} - V_{\phi_2})}{\rho_1 d_{\phi_1}^3 + \rho_{\phi_2} d_{\phi_2}^3}\right), \tag{C6}$$

where α_{ϕ_1} is the volume fraction of small particles, θ is the granular temperature of the small particles that is assumed to be 10% of the mean vertical particle velocity, e is a restitution coefficient that is approximately 0.51 based on experiments by *Dufek et al.* [2009], g_o is a radial distribution function, and we assume that it is approximately 1 because our current is very dilute. We use equations (C1)–(C6) to solve for V where $\frac{dV}{dt} = 0$, or particle terminal velocity, in our model.

Notation

e_n Splash Function restitution coefficient
N_e number of ejected particles
V_i impactor velocity
θ_i incidence angle
m_i impactor mass
m_e mass of an ejected particle
g gravitational acceleration
L characteristic length scale
d_c impact crater depth
μ tangent of the friction angle
ρ_i impactor density
ρ_e ejected particle density
d_i impactor diameter
d_e ejected particle diameter
h_i height from which the impactor is dropped
m_a mass of air per unit area
$m_{\phi 1}$ mass per unit area of the small particle fraction
$m_{\phi 2}$ mass per unit area of the large particle fraction
T_i initial temperature of particles in the PDC
T_a ambient temperature
T_c bulk temperature of the PDC
H thermal energy per unit area
C_p^a heat capacity of air
C_p^r heat capacity of rock
h PDC height
M molar mass of air
R universal gas constant
P atmospheric pressure
ρ_c bulk PDC density
u depth-averaged PDC velocity
ρ_a ambient density
g' reduced gravity
E entrainment rate
ρ_{ϕ_1} density of the small particle fraction
ρ_{ϕ_2} density of the large particle fraction
t time
x distance
m_i total mass of impactors
β Splash Function coefficient
V_{ϕ_1} settling velocity of the small particle fraction
V_{ϕ_2} settling velocity of the large particle fraction
T_e temperature of the entrained particles
t_r time when runout distance is reached
L_r runout distance
d particle diameter
a scaling factor
p power law exponent

V particle settling velocity
F_g force of gas
F_s force of many small particles
ρ_p particle density
ρ_g gas density
μ_g dynamic air viscosity
f empirical correction to drag coefficient
τ_p particle response time
α_{ϕ_1} volume fraction small particles
θ granular temperature of the small particles
e restitution coefficient
g_o radial distribution function

Acknowledgments
We thank Judy Webb for contributions that enabled this work. We are grateful for constructive comments and feedback from reviewers Olivier Roche and Jennie Gilbert and Editor Andre Revil, and we thank Olivier Roche for the suggestion in the last sentence of section 6.3. K.F. was supported by a NSF GRFP fellowship. Additional support was provided by NSFEAR1144198 and NSFEAR1447559. Data and code used in this study are available at https://vhub.org/resources/4068.

References

Anderson, R. S. (1987), A theoretical model for aeolian impact ripples, *Sedimentology*, *34*, 943–956, doi:10.1111/j.1365-3091.1987.tb00814.x.
Anderson, R. S., and P. K. Haff (1988), Simulation of eolian saltation, *Science*, *241*(4867), 820–823.
Andreotti, B. (2004), A two-species model of aeolian sand transport, *J. Fluid Mech.*, *510*, 47–70, doi:10.1017/S0022112004009073.
Andrews, B. J. (2014), Dispersal and air entrainment in unconfined dilute pyroclastic density currents, *Bull. Volcanol.*, *76*(9), 1–14.
Andrews, B. J., and M. Manga (2012), Experimental study of turbulence, sedimentation, and coignimbrite mass partitioning in dilute pyroclastic density currents, *J. Volcanol. Geotherm. Res.*, *225*, 30–44.
Beladjine, D., M. Ammi, L. Oger, and A. Valance (2007), Collision process between an incident bead and a three-dimensional granular packing, *Phys. Rev. E: Stat. Nonlinear Soft Matter Phys.*, *75*(6), 1–12, doi:10.1103/PhysRevE.75.061305.
Benage, M. C. (2015), The thermal evolution and dynamics of pyroclasts and pyroclastic density currents, PhD Thesis, Georgia Institute of Technology.
Benage, M. C., J. Dufek, and P. A. Mothers (2016), Quantifying entrainment in pyroclastic density currents from the Tungurahua eruption, Ecuador: Integrating field proxies with numerical simulations, *Geophys. Res. Lett.*, *43*, 1–10, doi:10.1002/2016GL069527.
Birch, S. P. D., M. Manga, B. Delbridge, and M. Chamberlain (2014), Penetration of spherical projectiles into wet granular media, *Phys. Rev. E: Stat. Nonlinear Soft Matter Phys.*, *90*(3), 1–8, doi:10.1103/PhysRevE.90.032208.
Brand, B. D., C. Mackaman-Lofland, N. M. Pollock, S. Bendaña, B. Dawson, and P. Wichgers (2014), Dynamics of pyroclastic density currents: Conditions that promote substrate erosion and self-channelization—Mount St Helens, Washington (USA), *J. Volcanol. Geotherm. Res.*, *276*, 189–214, doi:10.1016/j.jvolgeores.2014.01.007.
Branney, M., and R. Brown (2011), Impactoclastic density current emplacement of terrestrial meteorite-impact ejecta and the formation of dust pellets and accretionary lapilli: Evidence from Stac Fada, Scotland, *J. Geol.*, *119*(3), 275–292, doi:10.1086/659147.
Branney, M. J., and B. P. Kokelaar (2002), *Pyroclastic Density Currents and the Sedimentation of Ignimbrites*, vol. 27, Geological Society of London, Memoirs, U. K.
Buesch, D. C. (1992), Incorporation and redistribution of locally derived lithic fragments within a pyroclastic flow, *Geol. Soc. Am. Bull.*, *104*(9), 1193–1207, doi:10.1130/0016-7606(1992)104<1193:IAROLD>2.3.CO;2.
Burgisser, A., G. W. Bergantz, and R. E. Breidenthal (2005), Addressing complexity in laboratory experiments: The scaling of dilute multiphase flows in magmatic systems, *J. Volcanol. Geotherm. Res.*, *141*(3), 245–265, doi:10.1016/j.jvolgeores.2004.11.001.
Bursik, M., and A. W. Woods (1996), The dynamics and thermodynamics of large ash flows, *Bull. Volcanol.*, *58*(2–3), 175–193.
Calder, E. S., R. S. J. Sparks, and M. C. Gardeweg (2000), Erosion, transport and segregation of pumice and lithic clasts in pyroclastic flows inferred from ignimbrite at Lascar Volcano, Chile, *J. Volcanol. Geotherm. Res.*, *104*(1–4), 201–235, doi:10.1016/S0377-0273(00)00207-9.
Charbonnier, S. J., and R. Gertisser (2008), Field observations and surface characteristics of pristine block-and-ash flow deposits from the 2006 eruption of Merapi Volcano, Java, Indonesia, *J. Volcanol. Geotherm. Res.*, *177*(4), 971–982.
Cole, P., E. Calder, T. Druitt, R. Hoblitt, R. Robertson, R. Sparks, and S. Young (1998), Pyroclastic flows generated by gravitational instability of the 1996–97 lava dome of Soufriere Hills Volcano, Montserrat, *Geophys. Res. Lett.*, *25*(18), 3425–3428.
Dade, W. B., and H. E. Huppert (1995), A box model for non-entraining, suspension-driven gravity surges on horizontal surfaces, *Sedimentology*, *42*(3), 453–471.
Dellino, P., and L. La Volpe (2000), Structures and grain size distribution in surge deposits as a tool for modelling the dynamics of dilute pyroclastic density currents at La Fossa di Vulcano (Aeolian Islands, Italy), *J. Volcanol. Geotherm. Res.*, *96*(1–2), 57–78, doi:10.1016/S0377-0273(99)00140-7.
Denlinger, R. P. (1987), A model for generation of ash clouds by pyroclastic flows, with application to the 1980 eruptions at Mount St. Helens, Washington, *J. Geophys. Res.*, *92*(B10), 10,284–10,298.
Doronzo, D. M., G. A. Valentine, P. Dellino, and M. D. de Tullio (2010), Numerical analysis of the effect of topography on deposition from dilute pyroclastic density currents, *Earth Planet. Sci. Lett.*, *300*(1), 164–173.
Druitt, T., E. Calder, P. Cole, R. Hoblitt, S. Loughlin, G. Norton, L. Ritchie, R. Sparks, and B. Voight (2002), Small-volume, highly mobile pyroclastic flows formed by rapid sedimentation from pyroclastic surges at Soufrière Hills Volcano, Montserrat: An important volcanic hazard, *Mem. Geol. Soc. London*, *21*, 263–280.
Dufek, J., and G. W. Bergantz (2007), Suspended load and bed-load transport of particle-laden gravity currents: The role of particle-bed interaction, *Theor. Comput. Fluid Dyn.*, *21*(2), 119–145, doi:10.1007/s00162-007-0041-6.
Dufek, J., M. Manga, and M. Staedter (2007), Littoral blasts: Pumice-water heat transfer and the conditions for steam explosions when pyroclastic flows enter the ocean, *J. Geophys. Res.*, *112*, B11201, doi:10.1029/2006JB004910.
Dufek, J., J. Wexler, and M. Manga (2009), Transport capacity of pyroclastic density currents: Experiments and models of substrate-flow interaction, *J. Geophys. Res.*, *114*(11), 1–13, doi:10.1029/2008JB006216.
Dufek, J., T. E. Ongaro, and O. Roche (2015), Pyroclastic density currents: Processes and models, *Encycl. Volcanoes*, 631–648.

Dufek, J. (2016), The fluid mechanics of pyroclastic density currents, *Annu. Rev. Fluid Mech.*, *48*(1), 459–485, doi:10.1146/annurev-fluid-122414-034252.
Durán, O., P. Claudin, and B. Andreotti (2011), On aeolian transport: Grain-scale interactions, dynamical mechanisms and scaling laws, *Aeolian Res.*, *3*(3), 243–270, doi:10.1016/j.aeolia.2011.07.006.
Esposti-Ongaro, T., A. Clarke, B. Voight, A. Neri, and C. Widiwijayanti (2012), Multiphase flow dynamics of pyroclastic density currents during the May 18, 1980 lateral blast of Mount St. Helens, *J. Geophys. Res.*, *117*, B06208, doi:10.1029/2011JB009081.
Freundt, A. (1999), Formation of high-grade ignimbrites Part II. A pyroclastic suspension current model with implications also for low-grade ignimbrites, *Bull. Volcanol.*, *60*(7), 545–567, doi:10.1007/s004450050251.
Garcia, M., and G. Parker (1993), Experiments on the entrainment of sediment into suspension by a dense bottom current, *J. Geophys. Res.*, *98*(C3), 4793–4807.
Huppert, H. E., and J. E. Simpson (1980), The slumping of gravity currents, *J. Fluid Mech.*, *99*(4), 785–799.
Iverson, R. M., and C. Ouyang (2015), Entrainment of bed material by Earth-surface mass flows: Review and reformulation of depth-integrated theory, *Rev. Geophys.*, *53*(1), 27–58, doi:10.1002/2013RG000447.
Kieffer, S. W., and B. Sturtevant (1988), Erosional furrows formed during the lateral blast at Mt. St. Helens, May 18, 1980, *J. Geophys. Res.*, *93*(B12), 14,793–14,816, doi:10.1029/JB093iB12p14793.
Kok, J. F., E. J. R. Parteli, T. I. Michaels, and D. B. Karam (2012), The physics of wind-blown sand and dust, *Rep. Prog. Phys.*, *75*(10), 106901, doi:10.1088/0034-4885/75/10/106901.
Lube, G., E. Breard, S. Cronin, and J. Jones (2015), Synthesizing large-scale pyroclastic flows: Experimental design, scaling, and first results from PELE, *J. Geophys. Res. Solid Earth*, *120*(3), 1487–1502.
Mitha, S., M. Q. Tran, B. T. Werner, and P. K. Haff (1986), The grain-bed impact process in aeolian saltation, *Acta Mech.*, *63*(1–4), 267–278, doi:10.1007/BF01182553.
Neri, A., T. Esposti Ongaro, G. Macedonio, and D. Gidaspow (2003), Multiparticle simulation of collapsing volcanic columns and pyroclastic flow, *J. Geophys. Res.*, *108*(B4), 2202, doi:10.1029/2001JB000508.
Newhall, K. A., and D. J. Durian (2003), Projectile-shape dependence of impact craters in loose granular media., *Phys. Rev. E: Stat. Nonlinear Soft Matter Phys.*, *68*, 060301, doi:10.1103/PhysRevE.68.060301.
Oger, L., M. Ammi, A. Valance, and D. Beladjine (2008), Study of the collision of one rapid sphere on 3D packings: Experimental and numerical results, *Comput. Math. Appl.*, *55*(2), 132–148, doi:10.1016/j.camwa.2007.04.001.
Pollock, N. M., B. D. Brand, and O. Roche (2016), The controls and consequences of substrate entrainment by pyroclastic density currents at Mount St Helens, Washington (USA), *J. Volcanol. Geotherm. Res.*, *325*, 135–147, doi:10.1016/j.jvolgeores.2016.06.012.
Roche, O. (2015), Nature and velocity of pyroclastic density currents inferred from models of entrainment of substrate lithic clasts, *Earth Planet. Sci. Lett.*, *418*, 115–125.
Roche, O., Y. Niño, A. Mangeney, B. Brand, N. Pollock, and G. A. Valentine (2013a), Dynamic pore-pressure variations induce substrate erosion by pyroclastic flows, *Geology*, *41*(10), 1107–1110, doi:10.1130/G34668.1.
Roche, O., J. Phillips, and K. Kelfoun (2013b), Pyroclastic density currents, in *Modeling Volcanic Processes: The Physics and Mathematics of Volcanism*, edited by S. A. Fagents, T. K. Gregg, and R. M. Lopes, Cambridge Univ. Press, Cambridge.
Roche, O., D. C. Buesch, and A. Greg (2016), Slow-moving and far-travelled dense pyroclastic flows during the Peach Spring super-eruption, *Nat. Comm.*, *7*, 10890, doi:10.1038/ncomms10890.
Scarpati, C., and A. Perrotta (2012), Erosional characteristics and behavior of large pyroclastic density currents, *Geology*, *40*(11), 1035–1038, doi:10.1130/G33380.1.
Sparks, R., L. Wilson, and G. Hulme (1978), Theoretical modeling of the generation, movement, and emplacement of pyroclastic flows by column collapse, *J. Geophys. Res.*, *83*(B4), 1727–1739.
Sparks, R. S. J., R. T. Bonnecaze, H. E. Huppert, J. R. Lister, M. A. Hallworth, H. Mader, and J. Phillips (1993), Sediment-laden gravity currents with reversing buoyancy, *Earth Planet. Sci. Lett.*, *114*(2–3), 243–257, doi:10.1016/0012-821X(93)90028-8.
Sparks, R. S. J., M. C. Gardeweg, E. S. Calder, and S. J. Matthews (1997), Erosion by pyroclastic flows on Lascar Volcano, Chile, *Bull. Volcanol.*, *58*(7), 557–565, doi:10.1007/s004450050162.
Stroberg, W. T., M. Manga, and J. Dufek (2010), Heat transfer coefficients of natural volcanic clasts, *J. Volcanol. Geotherm. Res.*, *194*(4), 214–219.
Suzuki-Kamata, K. (1988), The ground layer of Ata pyroclastic flow deposit, southwestern Japan—Evidence for the capture of lithic fragments, *Bull. Volcanol.*, *50*, 119–129.
Todesco, M., A. Neri, T. E. Ongaro, P. Papale, G. Macedonio, R. Santacroce, and A. Longo (2002), Pyroclastic flow hazard assessment at Vesuvius (Italy) by using numerical modeling. I. Large-scale dynamics, *Bull Volcanol.*, *64*(3–4), 155–177.
Ungar, J. E., and P. K. Haff (1987), Steady state saltation in air, *Sedimentology*, *34*(2), 289–299, doi:10.1111/j.1365-3091.1987.tb00778.x.
Valentine, G. A., and B. Giannetti (1995), Single pyroclastic beds deposited by simultaneous fallout and surge processes: Roccamonfina volcano, Italy, *J. Volcanol. Geotherm. Res.*, *64*(1), 129–137.
Werner, B. (1990), A steady-state model of wind-blown sand transport, *J. Geol.*, *98*(1), 1–17.
Werner, B., and P. Haff (1986), A simulation study of the low energy ejecta resulting from single impacts in eolian saltation, in *Advancements in Aerodynamics, Fluid Mechanics and Hydraulics*, pp. 337–345, ASCE, New York.
Willetts, B. B., and M. A. Rice (1986), Collisions in aeolian saltation, *Acta Mech.*, *63*(1-4), 255–265, doi:10.1007/BF01182552.
Wu, C.-Y. (2013), An energy-based Splash Function for the impact of particles with granular beds, in *POWDERS AND GRAINS 2013: Proceedings of the 7th International Conference on Micromechanics of Granular Media*, vol. 1542, pp. 630–633, AIP Publ, Sydney, Australia.